# The 3309 cm$^{-1}$ Series in Sapphire and Ruby: A Focus on FTIR Peak Position Variation

Wasura Soonthorntantikul and Aaron C. Palke

**Heat treatment of some ruby and sapphire can be identified by detection of the 3309 cm$^{-1}$ series in their infrared spectra. The 3309 cm$^{-1}$ series consists of three peaks at 3309, 3232, and 3185 cm$^{-1}$, with two additional weak peaks at 3367 and 3295 cm$^{-1}$. Observation of this series in a ruby or sapphire has significantly different implications than the identification of a single peak at 3309 cm$^{-1}$. This series represents a specific form of hydrogen incorporation in the corundum structure that is a diagnostic indicator of heat treatment for certain types of ruby and sapphire, particularly ruby from Mozambique and pink sapphire from Madagascar. However, identification of this series can be challenging because other peaks can occur in the same region as the 3309 cm$^{-1}$ series. This article presents criteria for accurate identification of the three main peaks in the 3309 cm$^{-1}$ series by measuring their possible peak position ranges, allowing for separation from other possible unrelated peaks in this region. Measurements were made on heated and unheated natural and laboratory-grown blue sapphire and ruby from various origins. With increasing iron and/or chromium content, the positions of these three main peaks shifted narrowly, about 1.7 to 3.6 cm$^{-1}$, from minimum positions at 3308.9, 3231.2, and 3183.7 cm$^{-1}$. A positive linear relationship was observed between the positions of three main peaks in the 3309 cm$^{-1}$ series and concentrations of iron for blue sapphire or the sum of iron and chromium for ruby. These relationships are useful to determine whether peaks in this region actually represent the 3309 cm$^{-1}$ series or some other hydrogen-related species in the corundum structure. Additionally, peak widths in the 3309 cm$^{-1}$ series also broaden with increasing iron or the sum of iron and chromium concentrations.**

Fourier-transform infrared (FTIR) absorption spectroscopy is often useful for detecting heat treatment in corundum or, in some cases, for demonstrating the absence of any heat treatment process (e.g., Sripoonjan et al., 2016). The relevant infrared region is approximately 3000–3600 cm$^{-1}$, which is generally related to the stretching frequency of hydroxyl groups bound in the corundum ($\alpha$-$Al_2O_3$) structure as well as hydroxyl group–related mineral inclusions in the corundum host (e.g., Moon and Phillips, 1991; Smith, 1995; Beran and Rossman, 2006).

Of particular interest for gemologists is a series of three main sharp peaks at approximately 3309, 3232, and 3185 cm$^{-1}$ and two additional weak peaks at 3367 and 3295 cm$^{-1}$, together known as the 3309 cm$^{-1}$ series. This series is related to the stretching vibrations of hydroxyl groups locally associated with titanium ions in the corundum structure (Moon and Phillips, 1991) and is commonly observed in natural blue sapphire from basalt-related deposits that are transported to the earth's surface by hot molten rock, or magma, producing natural thermal annealing. Most importantly, this series can also be introduced or removed from corundum by artificial heat treatment (Emmett et al., 2003). The presence of at least two peaks at approximately 3309 and 3232 cm$^{-1}$ in the series has been considered diagnostic evidence of post-growth artificial heat treatment for metamorphic blue sapphire (e.g., Hughes and Perkins, 2019), ruby from some deposits (e.g., Smith, 1995; Krzemnicki, 2018; Vertriest and Saeseaw, 2019), and pink sapphire from Madagascar (e.g., Saeseaw et al., 2020). This can be especially helpful for identifying low-temperature heat

See end of article for About the Authors and Acknowledgments.
Gems & Gemology, Vol. 61, No. 1, pp. 2–15,
http://dx.doi.org/10.5741/GEMS.61.1.2

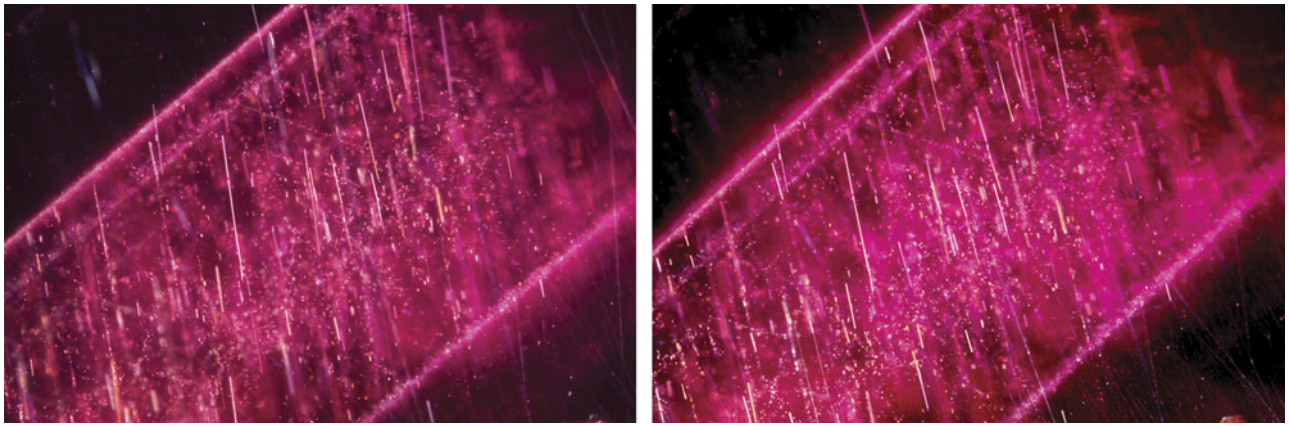

*Figure 1. This Mozambique ruby contains needles and bands of particles before heating (left). The inclusions did not show any signs of alteration after heating at 900°C for 5 hours in air (right). However, the development of the 3309 cm$^{-1}$ series in the FTIR spectrum was detected in this stone after heating, providing evidence of low-temperature heat treatment. Photomicrographs by Suwasan Wongchacree; field of view 1.75 mm.*

treatment, which often does not affect inclusions and leaves no microscopic clues (figure 1).

The concentration of hydroxyl groups in natural corundum is generally 0.5 ppmw or lower (Beran and Rossman, 2006). Previous work has reported various hydroxyl group stretching absorption features in FTIR spectra of natural and laboratory-grown corundum (Müller and Günthard, 1966; Belt, 1967; Eigenmann et al., 1972; Volynets et al., 1972; Engstrom et al., 1980; Beran, 1991; Moon and Phillips, 1991, 1994; Ramírez et al., 1997, 2004; Kronenberg et al., 2000; Beran and Rossman, 2006; Smith and van der Bogert, 2006). In addition to the 3309 cm$^{-1}$ series, other hydroxyl group–related absorption features with unknown origin have been documented in a similar region for both untreated and treated corundum, such as a peak at about 3220 cm$^{-1}$ and the acceptor-dominated 3000 cm$^{-1}$ series in untreated Montana sapphire (Palke et al., 2023), or several broad bands between 3050–3200 cm$^{-1}$ in sapphire treated with both heat and pressure (Soonthorntantikul et al., 2021). Incorporation of different trace elements in the corundum structure can produce variability in the position and width of some hydroxyl group–related absorption bands. For example, Beran (1991) reported FTIR peaks for variously colored laboratory-grown sapphires, including three narrow hydroxyl group bands at 3310, 3230, and 3185 cm$^{-1}$, with an additional narrow band at 3290 cm$^{-1}$ for some vanadium-, chromium-, iron-, and titanium-doped sapphires (color-change laboratory-grown sapphires) and a weak narrow band at 3280 cm$^{-1}$ for colorless sapphire. Volynets et al. (1972) reported broad hydroxyl group–related absorption bands at approximately 3000 cm$^{-1}$ for laboratory-grown sapphire doped with magnesium, also seen in laboratory-grown sapphire with cobalt and nickel as reported by Müller and Günthard (1966) and Eigenmann et al. (1972). Post-growth treatments of laboratory-grown materials, such as heat treatment (Moon and Phillips, 1991, 1994), hydrothermal treatment (Kronenberg et al., 2000), and electric field application with annealing (Ramírez et al., 2004), can alter the distribution of existing hydroxyl group band intensities or induce new hydroxyl group–related absorption features. Balan (2020) also performed density functional theory modeling and predicted the positions of various hydrogen-related species in the corundum structure. Additionally, in the gemological

## In Brief

- The 3309 cm$^{-1}$ series in FTIR spectra can be observed in unheated basalt-related blue sapphire, heated metamorphic blue sapphire and ruby, and laboratory-grown blue sapphire.
- Comparing the peak intensities between 3309 and 3232 cm$^{-1}$ in natural unheated and heated blue sapphire, the more intense peak is more commonly found at 3309 cm$^{-1}$ (3309 > 3232). In addition, the ratio of the peak intensities of the 3232 and 3185 cm$^{-1}$ absorption coefficient is generally around 3.
- The positions of the three main peaks in the 3309 cm$^{-1}$ series had a positive linear relationship with concentrations of iron and chromium. The widths of the peaks also slightly increase at higher iron and chromium concentrations.

laboratory, FTIR spectra are collected on a multitude of sapphires and rubies every year, and often peaks are observed that have not been described before in the literature, leaving their ultimate origin or meaning unknown.

All of this together could present a problem when determining whether a set of peaks in an FTIR spectrum of an unknown sapphire or ruby actually corresponds to the 3309 $cm^{-1}$ series in order to identify potential heat treatment. A further complication comes from the work of Phan (2015), who reported that the 3309 $cm^{-1}$ peak can shift position and identified a positive linear correlation between the position of the 3309 $cm^{-1}$ peak and iron concentrations. This raises the question of when a peak in the vicinity of the 3232 $cm^{-1}$ peak can be used as evidence of the presence of the 3309 $cm^{-1}$ series.

This article elaborates on the correlations between positions of the peaks in the 3309 $cm^{-1}$ series with trace element concentrations for ruby, metamorphic and basalt-related blue sapphire, and laboratory-grown sapphire. The aim of the work is to clarify when an FTIR feature can be considered evidence of the presence of the 3309 $cm^{-1}$ series.

## MATERIALS AND METHODS

**Samples.** A total of 659 samples of various types of blue sapphire and ruby were studied to cover a wide range of iron and chromium concentrations. This study set consisted of 395 untreated blue sapphires from basalt-related deposits, 52 untreated metamorphic blue sapphires, 63 laboratory-grown blue sapphires, 75 unheated rubies, and 74 heated rubies. The untreated blue sapphires from basalt-related and metamorphic deposits were selected from GIA's colored stone reference collection: 103 from Australia, 59 from Cambodia, 11 from Cameroon, 68 from Ethiopia, 74 from Nigeria, 29 from Thailand, and 51 from Vietnam for basalt-related deposits; and 9 from Myanmar (Burma), 21 from Madagascar, 12 from Sri Lanka, and 10 from Tanzania for metamorphic deposits. The rough samples were fabricated into wafers with a set of parallel polished surfaces that were either oriented (122 samples) or unoriented (325 samples) relative to the *c*-axis. The data for the laboratory-grown blue sapphires and unheated and heated rubies were extracted from the GIA database that analyzed these corundum samples from client submissions in faceted form. In the study, all selected samples showed at least one peak at 3309 $cm^{-1}$ by itself or a set of peaks at 3309, 3232, and/or 3185 $cm^{-1}$.

**Fourier-Transform Infrared (FTIR) Absorption Spectroscopy.** Unpolarized FTIR spectra were taken on all samples at room temperature using a Thermo Nicolet 6700 or iS50 FTIR spectrometer equipped with an XT-KBr beamsplitter and a cryogenic MCT detector operating with a 4× beam condenser accessory. Resolution was set at 2 or 4 $cm^{-1}$. Polarized spectra were recorded with an iS50 FTIR spectrometer, which included a motorized zinc selenide wire grid polarizer accessory. The intensities, positions, and widths of the absorption peaks were determined by fitting the spectra with Thermo Scientific's GRAMS/AI spectroscopy software using a multipoint linear baseline correction together with the combined Gaussian (*G*)-Lorentzian (*L*) function [expressed as $(1–M)^* G + M^*L$, where *M* is mixture (%Lorentzian)]. In terms of peak intensity, the spectra were converted to absorption coefficient ($\alpha$, $cm^{-1}$) using $\alpha = 2.303A/d$, where *A* is absorbance and *d* is path length in centimeters.

**Laser Ablation–Inductively Coupled Plasma–Mass Spectrometry (LA-ICP-MS).** Trace element chemistry was determined for all samples by LA-ICP-MS with a Thermo Fisher Scientific iCAP Q ICP-MS coupled with a Q-switched Nd:YAG laser ablation device operating at a wavelength of 213 nm. The laser conditions were set up with 55 μm diameter laser spots with fluence of approximately 10 $J/cm^2$ and a repetition rate of either 10 or 20 Hz. The dwell time was 40 seconds for each spot; the forward power was set at 1350 W, and the typical nebulizer gas flow was approximately 0.80 L/min. A special set of corundum reference standards was used for quantitative analysis of beryllium, magnesium, titanium, vanadium, chromium, iron, and gallium (Stone-Sundberg et al., 2017). NIST Standard Reference Materials 610 and 612 glasses were used for quantitative analysis of other elements. All elemental measurements were normalized on $^{27}Al$ as an internal elemental standard set at 529,250 ppmw with the following isotopes measured: $^{9}Be$, $^{24}Mg$, $^{47}Ti$, $^{51}V$, $^{53}Cr$, $^{57}Fe$, and $^{69}Ga$. Detection limits of measurable trace elements in corundum were 0.03–0.9 ppma magnesium, 0.3–1.5 ppma titanium, 0.01–0.2 ppma vanadium, 0.1–1.2 ppma chromium, 1–12 ppma iron, and 0.01–0.09 ppma gallium.

## RESULTS AND DISCUSSION

**Relative Intensity of Peaks at 3309, 3232, and 3185 $cm^{-1}$.** Focusing on the three main peaks at 3309, 3232,

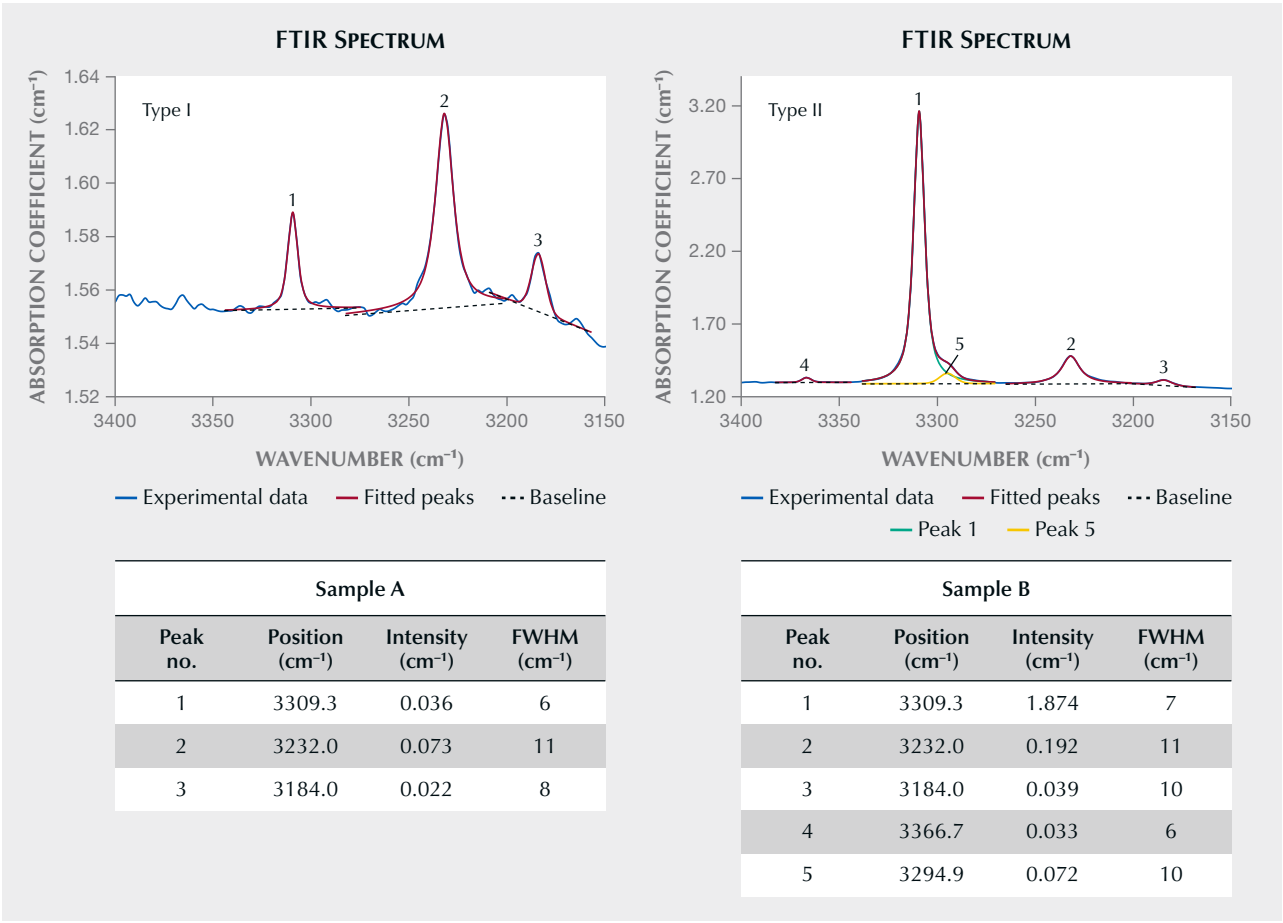


| Sample A | | | |
|---|---|---|---|
| Peak no. | Position ($cm^{-1}$) | Intensity ($cm^{-1}$) | FWHM ($cm^{-1}$) |
| 1 | 3309.3 | 0.036 | 6 |
| 2 | 3232.0 | 0.073 | 11 |
| 3 | 3184.0 | 0.022 | 8 |

| Sample B | | | |
|---|---|---|---|
| Peak no. | Position ($cm^{-1}$) | Intensity ($cm^{-1}$) | FWHM ($cm^{-1}$) |
| 1 | 3309.3 | 1.874 | 7 |
| 2 | 3232.0 | 0.192 | 11 |
| 3 | 3184.0 | 0.039 | 10 |
| 4 | 3366.7 | 0.033 | 6 |
| 5 | 3294.9 | 0.072 | 10 |

*Figure 2. Examples of unpolarized FTIR spectra of the studied samples showing the 3309 $cm^{-1}$ series for type I (left) and type II (right) according to Beran (1991). Sample A: Nigerian blue sapphire, wafer plane perpendicular to the* c*-axis, thickness 1.114 mm. Sample B: Cambodian blue sapphire, wafer plane parallel to the* c*-axis, thickness 1.036 mm. The peak fitting of the 3309 $cm^{-1}$ series is also illustrated using a multipoint linear baseline correction together with the combination of Gaussian and Lorentzian functions to fit peaks for measuring the positions, intensities, and full width at half maximum (FWHM). In the type II spectrum, a deconvolution of peak 5 that appears as a shoulder of peak 1 was also performed.*

and 3185 $cm^{-1}$ (excluding the peaks at 3367 and 3295 $cm^{-1}$), the majority of untreated basalt-related blue sapphires in this study (~85%) revealed this set of three main peaks at 3309, 3232, and/or 3185 $cm^{-1}$, and the remaining samples showed only a single peak at 3309 $cm^{-1}$. The crystalline defect producing the 3309 $cm^{-1}$ peak is attributed to hydroxyl groups associated with an aluminum vacancy and two tetravalent titanium ions ($Ti^{4+}$), whereas the defect producing the 3232 and 3185 $cm^{-1}$ peaks is related to hydroxyl groups with an aluminum vacancy and a single $Ti^{4+}$ in different configurations (Moon and Phillips, 1991, 1994). The peaks in the 3309 $cm^{-1}$ series are strongly polarized, with maximum absorption intensity when the electric field of incoming light is perpendicular to the *c*-axis (Beran, 1991; Moon and Phillips, 1991; Phan, 2015). According to Beran (1991), there are two types of patterns for the 3309 $cm^{-1}$ series based on the relative intensity (I) of the peaks at 3309 and 3232 $cm^{-1}$. Type I corundum has stronger absorption at 3232 $cm^{-1}$, while type II has stronger absorption at 3309 $cm^{-1}$. While Beran (1991) developed these types based on laboratory-grown sapphire, both types of the 3309 $cm^{-1}$ series can also be found in natural corundum (Phan, 2015). The distribution of hydroxyl group peak intensities at 3309, 3232, and 3185 $cm^{-1}$ depends on the final equilibrium temperature and thermal history of the sapphires (Moon and Phillips, 1991, 1994; Ramírez et al., 2004).

In this study, FTIR spectra of basalt-related blue sapphire samples displayed both type I and type II spectra (figure 2). Although the intensities of the three

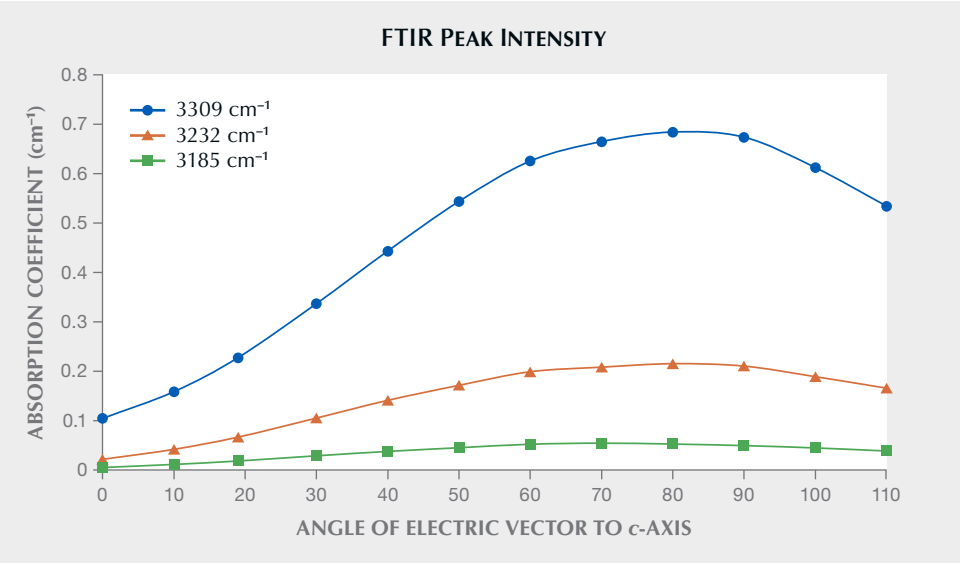


*Figure 3. Absorption coefficients (cm⁻¹) at various electric vector angles relative to the c-axis for 3309, 3232, and 3185 cm⁻¹ peaks in the 3309 cm⁻¹ series. Sample: Nigerian blue sapphire, wafer plane parallel to the c-axis, thickness 3.388 mm.*

main peaks varied with angles between the electric vector and the *c*-axis, the change in their peak intensities follows the same trends and their relative intensities remain the same, as shown in figure 3 and references therein. Unpolarized FTIR spectra of the studied samples can be used for further discussion on spectrum type/relative peak intensities for the 3309 cm$^{-1}$ series. In unheated basalt-related blue sapphire, type II (spectra with the intensity of the 3309 cm$^{-1}$ peak greater than the 3232 cm$^{-1}$ peak; 3309 > 3232) is more commonly found (>80%), whereas type I (spectra with intensity of the 3309 cm$^{-1}$ peak smaller than the 3232 cm$^{-1}$ peak; 3309 < 3232) and intermediate type (comparable intensities between 3309 and 3232) can be occasionally observed in material from Cambodia, Ethiopia, Nigeria, and Vietnam (figure 4). For other corundum types in the study, all of the laboratory-grown blue sapphires and a majority of the heated rubies (>90%) exhibit type II spectra for the 3309 cm$^{-1}$ series, whereas the remaining samples of heat-treated rubies show the 3309 cm$^{-1}$ series with intermediate type. The unheated natural metamorphic blue sapphires and unheated natural rubies show only a single peak at 3309 cm$^{-1}$.

With heat treatment, the intensity of the 3309 cm$^{-1}$ peak changes in the opposite direction to that of the 3232 and 3185 cm$^{-1}$ peaks (e.g., Moon and Phillips, 1991; Soonthorntantikul et al., 2019; Vertriest and

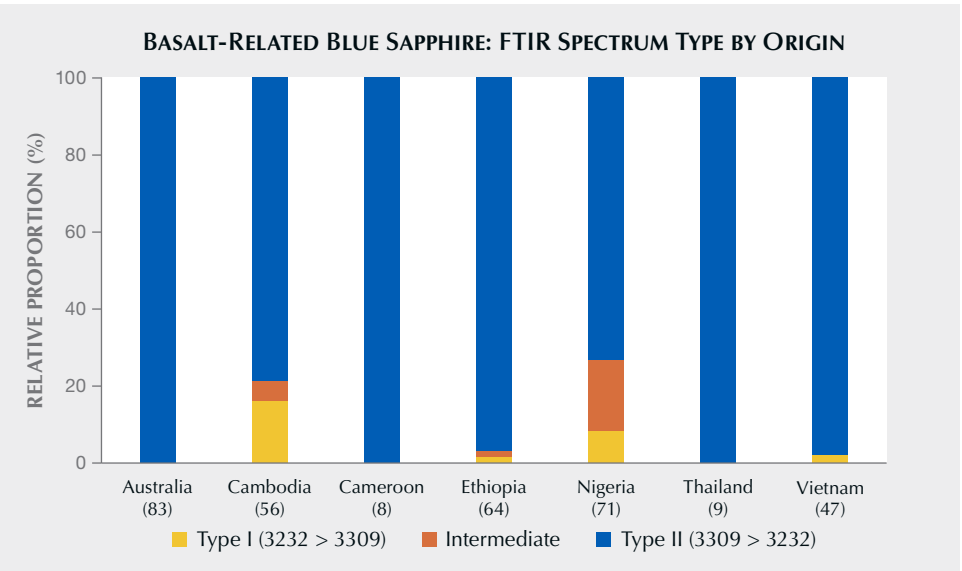


*Figure 4. The distribution of the unpolarized FTIR spectra of the 3309 cm⁻¹ series observed in unheated blue sapphires from various basalt-related deposits in this study. The numbers in parentheses represent the number of samples from each deposit.*

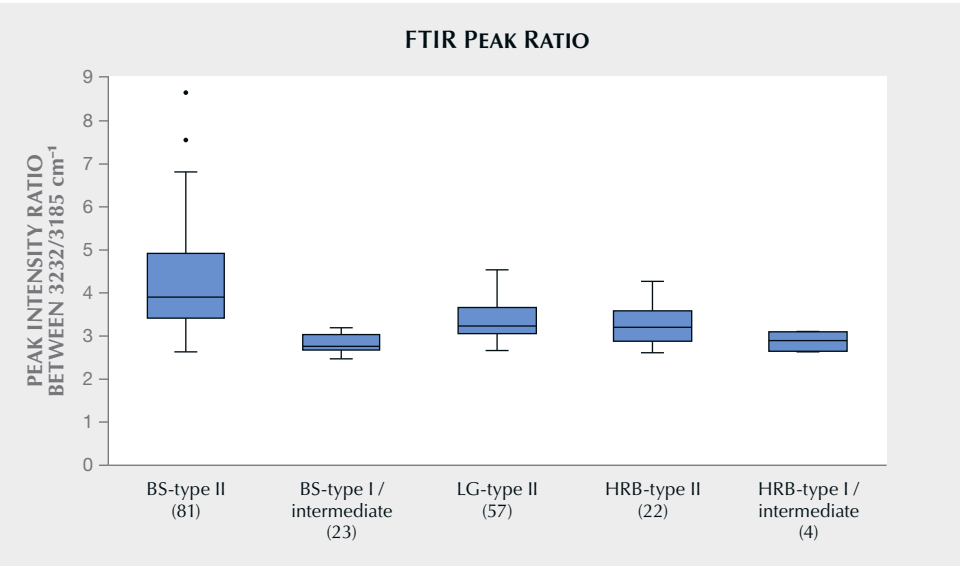


*Figure 5. The distribution of peak intensity ratio between 3232 and 3185 cm$^{-1}$ in different sample groups (extracted from unpolarized FTIR spectra): basalt-related blue sapphire (BS) with type II spectra, basalt-related blue sapphire with type I and intermediate spectra, laboratory-grown blue sapphire (LG) with type II spectra, heated ruby (HRB) with type II spectra, and heated ruby with type I and intermediate spectra. The numbers in parentheses represent the number of samples.*

Saeseaw, 2019; Saeseaw et al., 2020). Usually the 3309 cm$^{-1}$ peak decreases in intensity while the 3232 and 3185 cm$^{-1}$ peaks increase, although some rare exceptions have been noted. Heating temperatures and cooling rates can alter the relative intensity of the 3309 and 3232 cm$^{-1}$ peaks and may change the spectrum type (type I, type II, or intermediate) (e.g., Moon and Phillips, 1991; Kronenberg et al., 2000; Ramírez et al., 2004). In all corundum, the 3232 cm$^{-1}$ peak is more intense than the 3185 cm$^{-1}$ peak ($I_{3232} > I_{3185}$) (figure 5). Basalt-related blue sapphire with type I or intermediate spectra, laboratory-grown blue sapphire, and heated ruby all show a peak intensity ratio of approximately 3 for $I_{3232}/I_{3185}$, in agreement with laboratory-grown sapphire at thermal equilibrium from both Beran (1991) and Moon and Phillips (1991). The 3:1 intensity ratio for the 3232 and 3185 cm$^{-1}$ bands comes from the structural arrangement of defect clusters with three available titanium sites for the defect species related to the 3232 cm$^{-1}$ band and one site for the 3185 cm$^{-1}$ band (Moon and Phillips, 1991). A slight deviation from the ratio of 3 is due to measurement errors for the weak 3185 cm$^{-1}$ band. Basalt-related blue sapphire with type II spectra shows a great variability of the ratio $I_{3232}/I_{3185}$, ranging between 3 and 9. This may be caused by complexities in the defect structure and growth conditions for hydrogen incorporation in natural samples, in addition to inaccuracy in measuring the weak 3185 cm$^{-1}$ band.

**Relationship Between Peak Width and Position for the 3309, 3232, and 3185 cm$^{-1}$ Bands and Trace Element Concentrations.** IR peak positions and peak width of structural hydroxyl groups in corundum can be affected by the incorporation of different trace elements in the corundum lattice (e.g., Eigenmann et al., 1972; Volynets et al., 1972; Moon and Phillips, 1994; Phan, 2015). FTIR data collected with 4 cm$^{-1}$ resolution were used here for peak width consideration. The main triplet of peaks at 3309, 3232, and 3185 cm$^{-1}$ in the series are sharp peaks with full width at half maximum (FWHM) of less than 18 cm$^{-1}$ for basalt-related blue sapphire, 11 cm$^{-1}$ for laboratory-grown blue sapphire, and 19 cm$^{-1}$ for unheated and heated ruby (figure 6). The narrow width of these hydroxyl group stretching bands is associated with intramolecular hydroxyl group bonds (Moon and Phillips, 1991). As seen in figure 6, the FWHM of the 3309 cm$^{-1}$ peak is the narrowest among the three, and the width of the 3232 cm$^{-1}$ peak is slightly larger than that of the 3185 cm$^{-1}$ peak at similar iron concentrations. Laboratory-grown blue sapphires, which generally have much lower iron concentrations (<280 ppma), showed smaller widths of hydroxyl group peaks compared to those of natural blue sapphires from basalt-related deposits with relatively high iron (>750 ppma). As seen in figure 6, all the peaks in the 3309 cm$^{-1}$ series for blue sapphires became wider with increasing iron concentrations (figure 6A) but show no relation to chromium due to their low chromium concentrations (figure 6C). On the other hand, rubies contain significant concentrations of not only chromium but also iron, and a broadening of peak widths in the series can be noticeably influenced by both chromium (figure 6D) and iron (figure 6B). Therefore, the trend of peak widths in the 3309 cm$^{-1}$ series for individual rubies could be estimated from the plot based on total concentrations of iron and chromium (figure 6F).

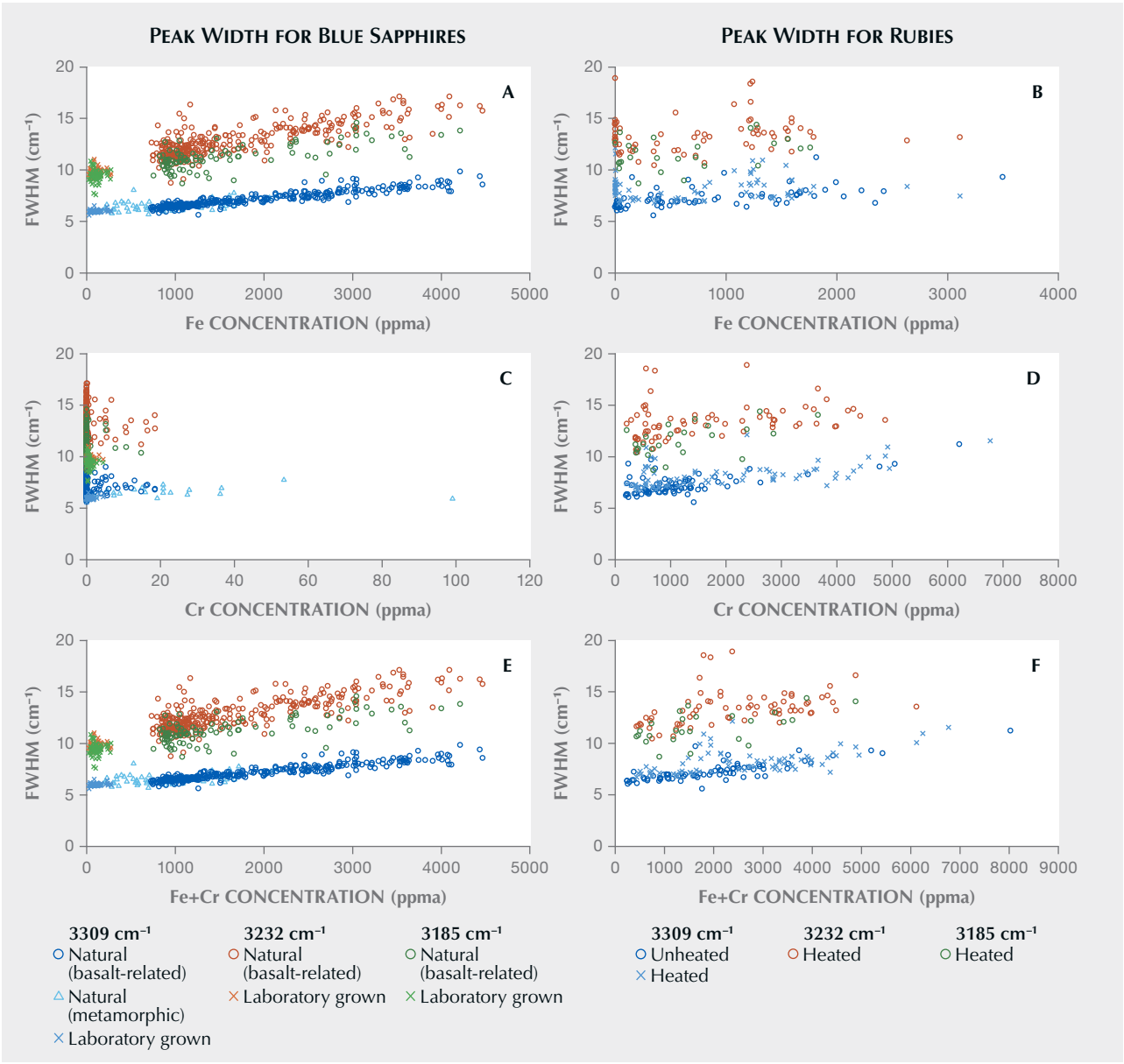


*Figure 6. The correlation of FWHM of the peaks at 3309, 3232, and 3185 cm$^{-1}$ with concentrations of iron (A and B), chromium (C and D), and the sum of iron and chromium (E and F) for blue sapphires (from metamorphic and basalt-related deposits as well as laboratory-grown material) and rubies. Resolution is 4 cm$^{-1}$ for all data presented here. See supplementary tables S1 and S2 at https://www.gia.edu/gems-gemology/spring-2025-ftir-3309-series-corundum.*

According to Phan (2015), variously colored natural sapphires from different localities revealed a peak at 3309 cm$^{-1}$ or a group of peaks including 3309 cm$^{-1}$, and a positive linear relationship was observed between peak position at 3310 cm$^{-1}$ (ranging from 3309 cm$^{-1}$ to 3311 cm$^{-1}$) and iron concentration (0.4 to 1.78 wt.% $Fe_2O_3$, or at approximately 1000 to 4500 ppma iron) in those sapphires. In this study, the samples were expanded to broader iron concentrations, ranging from 204 to 4465 ppma in natural sapphires and 22 to 275 ppma in laboratory-grown blue sapphires. Although IR peak intensities of the 3309 cm$^{-1}$ series change with polarization (Beran, 1991; Moon and Phillips, 1991), peak positions do not shift with polarization (standard deviation of ±0.01, ±0.1, and ±0.1 cm$^{-1}$ for 3309, 3232, and 3185 cm$^{-1}$, respectively, at various polarization angles).

Figure 7 shows the correlation between the measured positions of the peaks in the 3309 cm$^{-1}$ series (3309, 3232, and 3185 cm$^{-1}$) and iron concentrations

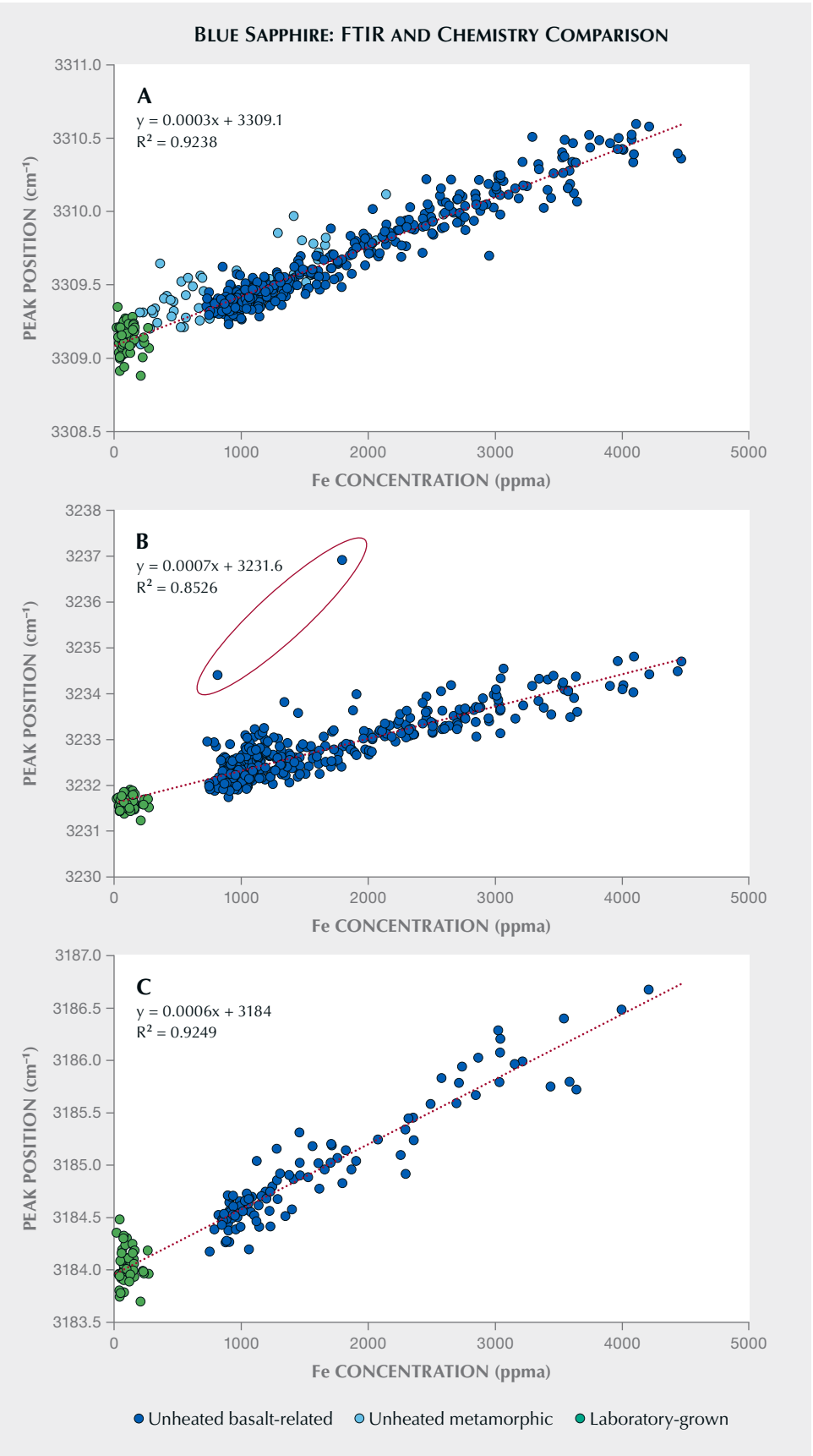


*Figure 7. The linear relationship (red dotted lines) between FTIR peak positions at 3309 (A), 3232 (B), and 3185 cm$^{-1}$ (C) in the 3309 cm$^{-1}$ series and iron concentrations for blue sapphires. In plot B, two outliers are contained in the red oval. See supplementary table S3 at https://www.gia.edu/gems-gemology/spring-2025-ftir-3309-series-corundum.*

in the natural and laboratory-grown blue sapphires. Laboratory-grown blue sapphire typically contains relatively low iron concentrations, as reflected in the study samples where iron was <280 ppma, and the measured peak position at 3309 $cm^{-1}$ of this group ranged between 3308.9 and 3309.3 $cm^{-1}$. There is no observable correlation between the peak position of the 3309 $cm^{-1}$ peak and iron concentration for laboratory-grown sapphires. This is due to the small range of iron concentration for these stones. For natural blue sapphires from metamorphic and basalt-related deposits in the study, the 3309 $cm^{-1}$ peak was observed between 3309.1 and 3310.6 $cm^{-1}$ for the samples with iron concentrations ranging from 204 to 4465 ppma. Although only the laboratory-grown sapphire data did not show any clear trend, the results acquired from natural and laboratory-grown sapphire groups align with each other. They showed a linear correlation of peak position at 3309 $cm^{-1}$ over a wide range of iron concentrations (figure 7A and table 1), which is consistent with Phan (2015).

In addition to the 3309 $cm^{-1}$ peak, the other two peaks at 3232 and 3185 $cm^{-1}$ showed similar correlation of peak positions over a wide range of iron concentrations for natural and laboratory-grown blue sapphires (figures 7B and 7C and table 1). The peak at 3232 $cm^{-1}$ varied from 3231.2 to 3234.8 $cm^{-1}$ (excluding two outliers in the plots at 3234.4 and 3236.9 $cm^{-1}$), while the peak at 3185 $cm^{-1}$ ranged between 3183.7 and 3186.7 $cm^{-1}$.

FTIR spectra of two outlier samples in the 3232 $cm^{-1}$ plot are shown in figure 8. In both cases, a cursory

**TABLE 1.** Parameters of linear regression function of individual hydroxyl group stretching peaks for sapphire and ruby data in figures 7 and 9, respectively.

| | 3309 $cm^{-1}$ | 3232 $cm^{-1}$[a] | 3185 $cm^{-1}$ |
|---|---|---|---|
| | Blue sapphire | | |
| Samples | 510 | 397 | 161 |
| $R^2$ | 0.92 | 0.85 | 0.92 |
| Standard error | 0.10 | 0.29 | 0.18 |
| Intercept | 3309.1 | 3231.6 | 3184.0 |
| Slope | $3.4\times10^{-4}$ | $7.0\times10^{-4}$ | $6.2\times10^{-4}$ |
| Observed peak frequencies | 3308.9–3310.6 | 3231.2–3234.8 | 3183.7–3186.7 |
| Iron concentration (in ppma) | 22–4465 | 22–4465 | 22–4465 |
| | Ruby | | |
| Samples | 149 | 70 | 25 |
| $R^2$ | 0.84 | 0.75 | 0.84 |
| Standard error | 0.17 | 0.32 | 0.25 |
| Intercept | 3309.1 | 3231.9 | 3184.4 |
| Slope | $2.8\times10^{-4}$ | $4.3\times10^{-4}$ | $4.5\times10^{-4}$ |
| Observed peak frequencies | 3308.9–3311.5 | 3231.8–3234.4 | 3184.4–3186.7 |
| Sum of iron and chromium concentrations (in ppma) | 240–8025 | 240–8025 | 240–8025 |

[a]*Two outliers in figure 7 are omitted.*

inspection of the spectra might lead one to use the peaks at 3234.4 or 3236.9 $cm^{-1}$ as evidence of the 3309 $cm^{-1}$ series and therefore an indicator of heat treatment. However, the significant deviations of their positions should give cause for caution in this interpretation. In fact, in one sample, the peak is far outside the observed range for the 3232 $cm^{-1}$ peak of 3231.2 to 3234.8 $cm^{-1}$. For the other sample, the peak is in the known range for the 3232 $cm^{-1}$ peak, but this peak position would only be observed at much higher iron concentrations than measured in this sample. (The standard deviation of 12 data points in this sample is less than 9% for iron concentration with measurements on both sides of the sample.) Both samples have similar FTIR patterns (figure 8): a doublet of peaks at 3379 and 3394 $cm^{-1}$ and a peak at 3309.7 $cm^{-1}$ for sample A and at 3309.3 $cm^{-1}$ for sample B. Of importance, with iron concentrations of 1795 ppma for sample A and 815 ppma for sample B, the positions of the peaks at 3309 $cm^{-1}$ align with the linear correlation shown in figure 7A. Finally, there is no observable peak at 3185 $cm^{-1}$. These observations indicate that the 3236.9 $cm^{-1}$ or 3234.4 $cm^{-1}$ peaks in both samples are not related to the 3309 $cm^{-1}$ series, especially considering that the 3236.9 $cm^{-1}$ peak is outside the possible range of 3231.2–3234.8 $cm^{-1}$ seen in figure 7B. Similar spectra have been seen in other stones submitted to the GIA laboratory, with a doublet at 3379/3394 $cm^{-1}$ as well as a smaller peak around 3235 $cm^{-1}$. It is possible that the peaks at 3234.4 and 3236.9 $cm^{-1}$ in these samples are part of another unidentified series together with the 3379/3394 $cm^{-1}$ doublet. Importantly, there is no evidence of a 3309 $cm^{-1}$ series in the FTIR spectra in figure 8.

Unlike for iron, in blue sapphire there is no correlation between peak positions for the 3309 $cm^{-1}$ series and other measurable trace elements, including titanium, vanadium, chromium, and gallium. This may be because these other trace elements are present at relatively low concentrations in blue sapphire. FTIR spectra of the basalt-related blue sapphires in this study also show other narrow peaks together with the 3309 $cm^{-1}$ series peaks, such as doublet peaks at approximately 3379 and 3394 $cm^{-1}$ (16% of the studied samples), a weak 3265 $cm^{-1}$ peak (5%), a weak 3210 $cm^{-1}$ peak (5%), a weak 3278 $cm^{-1}$ peak (2%), and a weak 3165 $cm^{-1}$ peak (less than 1%). Among these additional peaks, it is notable that the weak

*Figure 8. FTIR spectra of two blue sapphires with the peak at approximately 3232 $cm^{-1}$ falling significantly outside a linear trend between peak frequency and iron concentrations in figure 7B. It is possible that the peaks at 3237 and 3234 $cm^{-1}$ in both spectra are not related bands in the 3309 $cm^{-1}$ series. The peaks at 3379 and 3394 $cm^{-1}$ with unknown defect origins are also present in both spectra. Sample A: Nigerian blue sapphire, unoriented, thickness 2.89 mm (left). Sample B: Cameroon blue sapphire, wafer plane parallel to the* c*-axis, thickness 3.923 mm (right).*

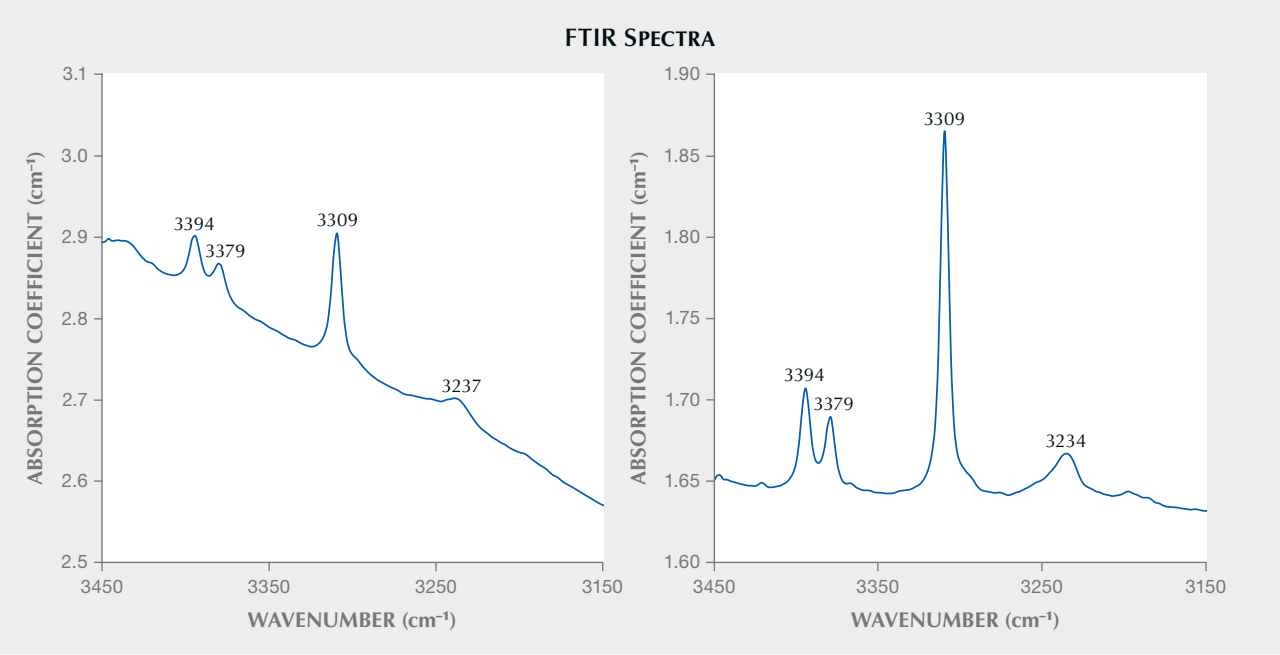

3210 $cm^{-1}$ peak is usually found in type I and type II spectra with relatively strong 3232 $cm^{-1}$ peak intensity (>25% of the 3309 $cm^{-1}$ intensity).

Blue sapphires typically contain low chromium concentrations, and the peak position shift within the 3309 $cm^{-1}$ series correlates solely with iron concentrations. In rubies, chromium is present at relatively high concentrations in addition to iron, which can vary from very low to high concentrations. Therefore, it is likely that both iron and chromium can have an impact on a peak position variation for the 3309 $cm^{-1}$ series in rubies when they are present at significant concentrations.

FTIR spectra and trace element chemistry of the natural rubies were measured to determine the relationship between peak positions in the 3309 $cm^{-1}$ series and concentrations of iron and chromium. The studied ruby samples, either untreated or heated, contain a wide range of iron and chromium concentrations: 195–6765 ppma chromium, 0–3497 ppma iron, and 240–8025 ppma for the sum of chromium and iron. The shift of peak position toward higher wavenumbers was observed at higher chromium or iron concentrations with a certain degree of linear correlation, for example, $R^2$ of 0.56 and 0.16 for the plots of the 3309 $cm^{-1}$ peak against concentrations of chromium and iron, respectively. Unlike blue sapphires, unheated and heated rubies showed a linear correlation between the positions of the peaks in the 3309 $cm^{-1}$ series and the sum of chromium and iron concentrations, with $R^2 > 0.75$ for three peaks in the series (figure 9, opposite page and table 1). The relationship between peak positions at approximately 3309, 3232, or 3185 $cm^{-1}$ and the sum of chromium and iron concentrations in natural rubies (figure 9 and table 1) follow the same trend as those in blue sapphires at various iron concentrations (figure 7 and table 1). The data plotted in figures 6, 7, and 9 are available in the supplementary data sheet at https://www.gia.edu/gems-gemology/spring-2025-ftir-3309-series-corundum.

As demonstrated above, high concentrations of either iron or chromium can produce a small shift of peak positions at 3309, 3232, and 3185 $cm^{-1}$ toward higher wavenumbers and also a slight broadening of the widths of these peaks. This may be caused by the larger ionic radius of $Fe^{3+}$ and $Cr^{3+}$ than $Al^{3+}$ [0.645 Å for $Fe^{3+}$, 0.615 Å for $Cr^{3+}$, and 0.535 Å for $Al^{3+}$ in an octahedral site (Shannon, 1976)]. In comparison with Al-O bond lengths [1.86 and 1.97 Å in $\alpha$-$Al_2O_3$ (Wyckoff, 1963)], longer bond distances for Fe-O [1.90 and 2.05 Å in $\alpha$-$Al_2O_3$: $Fe^{3+}$ (Gaudry et al., 2003)] and Cr-O [1.92 and 2.01 Å in $\alpha$-$Al_2O_3$: $Cr^{3+}$ (Gaudry et al., 2003)] result in weaker cation-oxygen interactions from surrounding environments of hydroxyl groups, and therefore, intramolecular OH stretching strengthens and shifts toward higher frequencies.

**Identification of the 3309 $cm^{-1}$ Series for the Stones with Unknown Treatment.** Several important conclusions can be made regarding the identification of the 3309 $cm^{-1}$ series when looking for evidence of heat treatment in ruby and sapphire:

- The peaks in the 3309 $cm^{-1}$ series do shift position but over a relatively narrow range.
- Peaks identified near the 3309, 3232, and 3185 $cm^{-1}$ peaks but outside the ranges prescribed here cannot be considered evidence of the 3309 $cm^{-1}$ series, and thus those peaks should not be used as evidence of heat treatment.
- The 3185 $cm^{-1}$ peak is observed only when there is also a 3232 $cm^{-1}$ peak that is at least three times more intense than the 3185 $cm^{-1}$ peak. A peak in the vicinity of the 3185 $cm^{-1}$ peak without a 3232 $cm^{-1}$ peak is not part of the 3309 $cm^{-1}$ series and should not be used as evidence of heat treatment.
- If trace element measurements are available, they can be used along with the relationships outlined here to determine if certain peaks may be part of the 3309 $cm^{-1}$ series.

Figure 10 provides an excellent example of these concepts, showing the FTIR spectrum of a ruby sub-

*Figure 10. FTIR spectrum of a ruby submitted to the GIA laboratory. The presence of a peak at 3180 $cm^{-1}$ was not considered evidence of heat treatment in this case because it is outside the range of possible positions for the 3185 $cm^{-1}$ peak. The absence of a 3232 $cm^{-1}$ peak also rules out the presence of the 3309 $cm^{-1}$ series.*

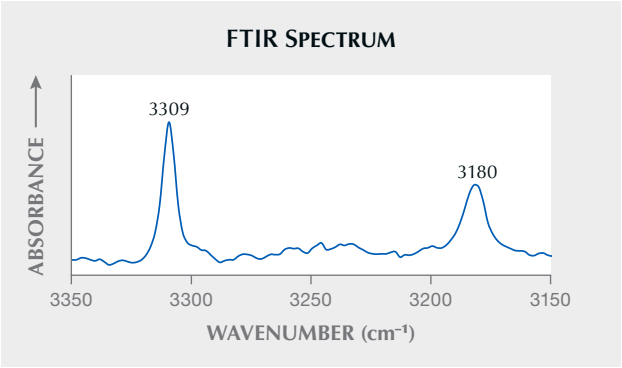

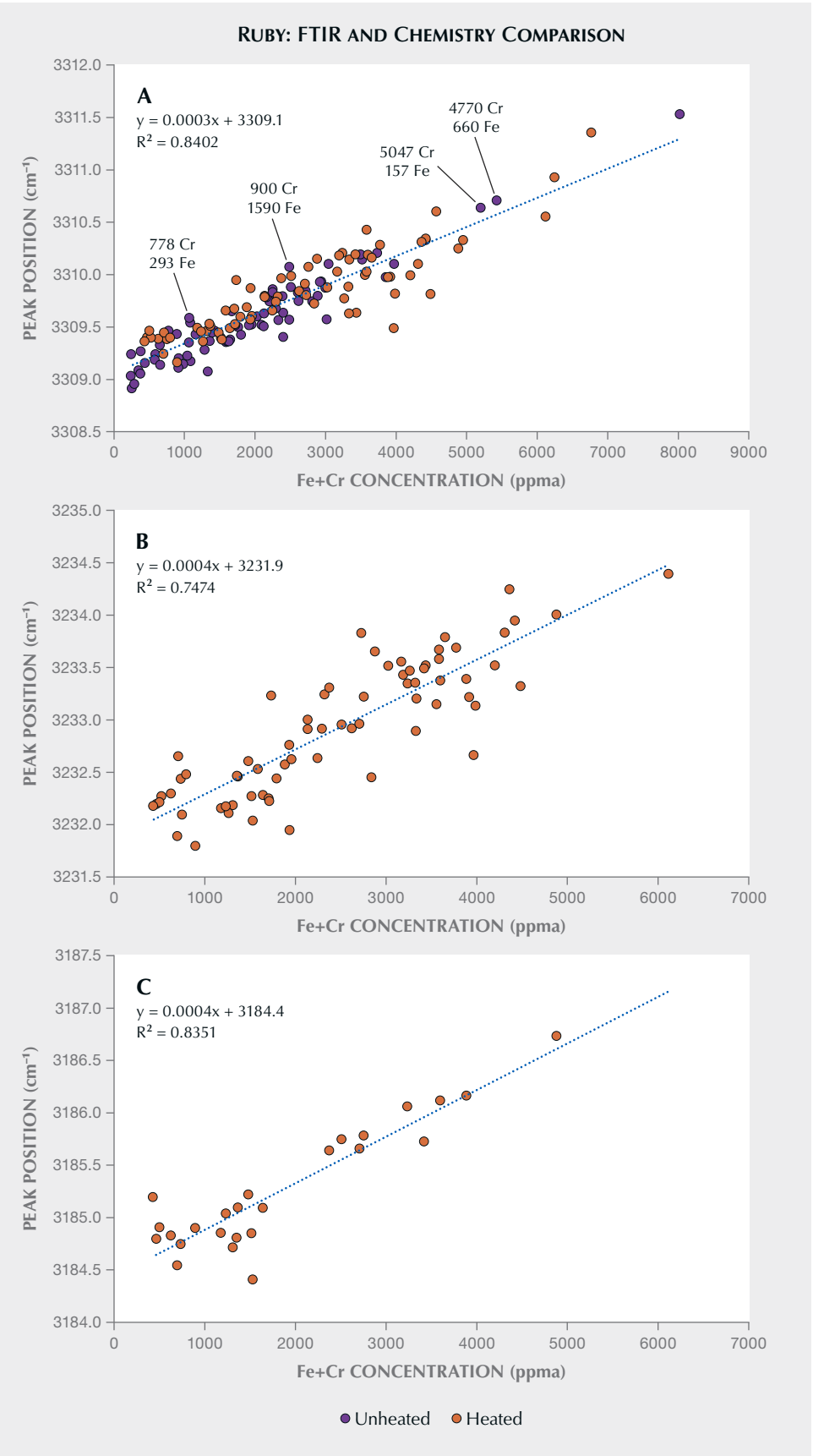


*Figure 9. The linear relationship (blue dotted lines) of FTIR peak positions at 3309 (A), 3232 (B), and 3185 $cm^{-1}$ (C) and the sum of iron and chromium concentrations for rubies. In plot A, some points are noted to show that in some cases the chromium and iron concentrations separately are not linearly correlated with the 3309 $cm^{-1}$ peak position. The combination of iron and chromium can affect the peak frequency shift in rubies. See supplementary table S4 at https://www.gia.edu/gems-gemology/spring-2025-ftir-3309-series-corundum.*

mitted to the GIA laboratory for an identification report. This spectrum shows a 3309 $cm^{-1}$ peak as well as a peak at 3180 $cm^{-1}$. The second is near where one may expect to see a 3185 $cm^{-1}$ peak, but it is out of range for that peak, especially considering that this feature only shifts up in position and would never shift down. Additionally, the absence of a peak at 3232 $cm^{-1}$ demonstrates that this peak at 3180 $cm^{-1}$ cannot be used as evidence of heat treatment.

## CONCLUSIONS

The 3309 $cm^{-1}$ series in FTIR, consisting of three main peaks at approximately 3309, 3232, and 3185 $cm^{-1}$, is associated with hydroxyl group stretching in titanium-bearing corundum. FTIR spectral parameters including relative intensity, peak width, and peak position were studied for different types of blue sapphire and ruby with a wide variety of trace element chemical compositions (figure 11). Considering the relative peak intensities of the 3309 $cm^{-1}$ series within the FTIR spectra of untreated natural blue sapphires, we found that the strongest peak is more commonly found at 3309 $cm^{-1}$ than at 3232 $cm^{-1}$. All of the samples in this study exhibited a 3232 $cm^{-1}$ peak of greater intensity than the peak at 3185 $cm^{-1}$. The ratio of the peak intensities of the 3232 and 3185 $cm^{-1}$ absorption coefficients in basalt-related blue sapphires with type I and intermediate spectra, laboratory-grown blue sapphires, and heated rubies was determined to be approximately 3, whereas basalt-related blue sapphires with type II spectra had a broader range of ratio values (3 to 9). The peak widths of the three main peaks in the 3309 $cm^{-1}$ series broadened with increasing concentrations of iron in blue sapphires and total chromium plus iron in rubies. A slight variation of peak positions at approximately 3309, 3232, and 3185 $cm^{-1}$ was observed at different concentrations of major trace elements in sapphire and ruby. These peaks shifted linearly toward higher wavenumbers from the minimum positions at 3308.9, 3231.2, and 3183.7 $cm^{-1}$ with increasing iron concentrations for blue sapphires, and increasing sum of chromium and iron concentrations for rubies. A correlation between triplet peaks in the 3309 $cm^{-1}$ series and iron (in blue sapphires) or the sum of iron and chromium (in rubies) can be useful to determine whether the 3309 $cm^{-1}$ series is present in an FTIR spectrum.

*Figure 11. Various types of corundum (ranging from 1.16 to 33.16 ct) that can present the 3309 $cm^{-1}$ series in FTIR spectra: unheated basalt-related blue sapphire (two stones in the bottom row), heated metamorphic blue sapphire (two stones in the top row), and pink sapphire and ruby. Photos by Robert Weldon, Orasa Weldon, Vincent Pardieu, Emily Lane, and Tino Hammid; stones courtesy of B&B Fine Gems, Kenneth Kin Ming Siu, and Joao Jose Ip Lau Tchun.*

ABOUT THE AUTHORS
*Dr. Wasura Soonthorntantikul is a research scientist at GIA in Bangkok. Dr. Aaron Palke is senior manager of research at GIA in Carlsbad, California.*

ACKNOWLEDGMENTS
*The authors thank many GIA colleagues for their valuable assistance with sample preparation and FTIR and LA-ICP-MS data collection, as well as Sudarat Saeseaw and Wim Vertriest for providing helpful comments and suggestions on an early version of the manuscript. We also thank the peer reviewers for their constructive feedback.*

## REFERENCES

Balan E. (2020) Theoretical infrared spectra of OH defects in corundum ($\alpha$-$Al_2O_3$). *European Journal of Mineralogy*, Vol. 32, No. 5, pp. 457–467, http://dx.doi.org/10.5194/ejm-32-457-2020

Belt R.F. (1967) Hydrothermal ruby: Infrared spectra and X-ray topography. *Journal of Applied Physics*, Vol. 38, No. 6, pp. 2688–2689, http://dx.doi.org/10.1063/1.1709972

Beran A. (1991) Trace hydrogen in Verneuil-grown corundum and its colour varieties—an IR spectroscopic study. *European Journal of Mineralogy*, Vol. 3, No. 6, pp. 971–976.

Beran A., Rossman G.R. (2006) OH in naturally occurring corundum. *European Journal of Mineralogy*, Vol. 18, No. 4, pp. 441–447, http://dx.doi.org/10.1127/0935-1221/2006/0018-0441

Eigenmann K., Kurtz K., Günthard Hs. H. (1972) Solid state reactions and defects in doped Verneuil sapphire. III. Systems $\alpha$-$Al_2O_3$: Fe, $\alpha$-$Al_2O_3$: Ti and $\alpha$-$Al_2O_3$: (Fe, Ti). *Helvetica Physica Acta*, Vol. 45, pp. 452–480.

Emmett J.L., Scarratt K., McClure S.F., Moses T., Douthit T.R., Hughes R., Novak S., Shigley J.E., Wang W., Bordelon O., Kane R.E. (2003) Beryllium diffusion of ruby and sapphire. *G&G*, Vol. 39, No. 2, pp. 84–135.

Engstrom H., Bates J.B., Wang J.C., Abraham M.M. (1980) Infrared spectra of hydrogen isotopes in $\alpha$-$Al_2O_3$. *Physical Review B*, Vol. 21, No. 4, pp. 1520–1526, http://dx.doi.org/10.1103/PhysRevB.21.1520

Gaudry E., Kiratisin A., Sainctavit P., Brouder C., Mauri F., Ramos A., Rogalev A., Goulon J. (2003) Structural and electronic relaxations around substitutional $Cr^{3+}$ and $Fe^{3+}$ ions in corundum. *Physical Review B*, Vol. 67, pp. 094108-1–094108-10, http://dx.doi.org/10.1103/PhysRevB.67.094108

Hughes E.B., Perkins R. (2019) Madagascar sapphire: Low-temperature heat treatment experiments. *G&G*, Vol. 55, No. 2, pp. 184–197, http://dx.doi.org/10.5741/GEMS.55.2.184

Krzemnicki M.S. (2018) New research by SSEF studies methods for detecting low-temperature heated rubies from Mozambique. Swiss Gemmological Institute, https://www.ssef.ch/wp-content/uploads/2018/09/SSEF-PRESS-RELEASE-New-research-by-SSEF-studies-methods-for-detecting-low-temperature-heated-rubies.pdf

Kronenberg A.K., Castaing J., Mitchell T.E., Kirby S.H. (2000) Hydrogen defects in $\alpha$-$Al_2O_3$ and water weakening of sapphire and alumina ceramics between 600 and 1000°C: I. Infrared characterization of defects. *Acta Materialia*, Vol. 48, No. 7, pp. 1481–1494, http://dx.doi.org/10.1016/S1359-6454(99)00448-6

Moon A.R., Phillips M.R. (1991) Defect clustering in H,Ti: $\alpha$-$Al_2O_3$. *Journal of Physics and Chemistry of Solids*, Vol. 52, No. 9, pp. 1087–1099, http://dx.doi.org/10.1016/0022-3697(91)90042-X

——— (1994) Defect clustering and color in Fe,Ti: $\alpha$-$Al_2O_3$. *Journal of the American Ceramic Society*, Vol. 77, No. 2, pp. 356–367, http://dx.doi.org/10.1111/j.1151-2916.1994.tb07003.x

Müller R., Günthard Hs. H. (1966) Spectroscopic study of the reduction of nickel and cobalt ions in sapphire. *Journal of Chemical Physics*, Vol. 44, No. 1, pp. 365–373, http://dx.doi.org/10.1063/1.1726471

Palke A.C., Renfro N.D., Hapeman J.R., Berg R.B. (2023) Gemological characterization of Montana sapphire from the secondary deposits at Rock Creek, Missouri River, and Dry Cottonwood Creek. *G&G*, Vol. 59, No. 1, pp. 2–45, http://dx.doi.org/10.5741/GEMS.59.1.2

Phan D.T.M. (2015) Internal characteristics, chemical compounds and spectroscopy of sapphire as single crystals. Doctoral dissertation, University of Johannes Gutenburg Mainz, https://d-nb.info/1075170532/34

Ramírez R., González R., Colera I., Vila R. (1997) Protons and deuterons in magnesium-doped sapphire crystals. *Journal of the American Ceramic Society*, Vol. 80, No. 4, pp. 847–850, http://dx.doi.org/10.1111/j.1151-2916.1997.tb02913.x

Ramírez R., Colera I., González R., Chen Y., Kokta M.R. (2004) Hydrogen-isotope transport induced by an electric field in $\alpha$-$Al_2O_3$ single crystals. *Physical Review B*, Vol. 69, article no. 041302, http://dx.doi.org/10.1103/PhysRevB.69.014302

Saeseaw S., Khowpong C., Vertriest W. (2020) Low-temperature heat treatment of pink sapphires from Ilakaka, Madagascar. *G&G*, Vol. 56, No. 4, pp. 448–457, http://dx.doi.org/10.5741/GEMS.56.4.448

Shannon R.D. (1976) Revised effective ionic radii and systematic studies of interatomic distances in halides and chalcogenides. *Acta Crystallographica*, Vol. A32, pp. 751–767, http://dx.doi.org/10.1107/S0567739476001551

Smith C.P. (1995) A contribution to understanding the infrared spectra of rubies from Mong Hsu, Myanmar. *Journal of Gemmology*, Vol. 24, No. 5, pp. 321–335.

Smith C.P., van der Bogert C. (2006) Infrared spectra of gem corundum. *G&G*, Vol. 42, No. 3, pp. 92–93.

Soonthorntantikul W., Saeseaw S., Palke A., McClure S. (2021) Gem News Internationl: FTIR observation on sapphires treated with heat and pressure. *G&G*, Vol. 57, No. 3, pp. 283–286.

Soonthorntantikul W., Khowpong C., Atikarnsakul U., Saeseaw S., Sangsawong S., Vertriest W., Palke A. (2019) Observations on the heat treatment of basalt-related blue sapphires. *GIA Research News*, May 1, https://www.gia.edu/gia-news-research/observations-heat-treatment-of-basalt-related-blue-sapphires

Sripoonjan T., Wanthanachaisaeng B., Leelawatanasuk T. (2016) Phase transformation of epigenetic iron staining: Indication of low-temperature heat treatment in Mozambique ruby. *Journal of Gemmology*, Vol. 35, No. 2, pp. 156–161.

Stone-Sundberg J., Thomas T., Sun Z., Guan Y., Cole Z., Equall R., Emmett J.L. (2017) Accurate reporting of key trace elements in ruby and sapphire using matrix-matched standards. *G&G*, Vol. 53, No. 4, pp. 438–451, http://dx.doi.org/10.5741/GEMS.53.4.438

Vertriest W., Saeseaw S. (2019) A decade of ruby from Mozambique: A review. *G&G*, Vol. 55, No. 2, pp. 162–183, http://dx.doi.org/10.5741/GEMS.55.2.162

Volynets F.K., Sidorova E.A., Stsepuro N.A. (1972) OH groups in corundum crystals which were grown with the Verneuil technique. *Journal of Applied Spectroscopy*, Vol. 17, pp. 1626–1628.

Wyckoff R.W.G. (1963) *Crystal Structures*, Vol. 1, 2nd ed. John Wiley and Sons, New York, p. 7.